ANNUAL REVIEWS

Annual Review of Materials Research

Low-Density, High-Temperature Co Base Superalloys

Surendra Kumar Makineni,[1,*]
Mahander Pratap Singh,[2,*]
and Kamanio Chattopadhyay[1,2]

[1]Department of Materials Engineering, Indian Institute of Science, Bangalore 560012, India; email: skmakineni@iisc.ac.in, kamanio@iisc.ac.in

[2]Interdisciplinary Centre for Energy Research, Indian Institute of Science, Bangalore 560012, India; email: mahanderp@iisc.ac.in

Annu. Rev. Mater. Res. 2021. 51:187–208

First published as a Review in Advance on June 3, 2021

The *Annual Review of Materials Research* is online at matsci.annualreviews.org

https://doi.org/10.1146/annurev-matsci-080619-014459

*These authors contributed equally to this article

Keywords

superalloys, solvus temperature, high-temperature strength, coarsening, creep

Abstract

Co base superalloys strengthened by coherent $L1_2$ ordered γ' precipitate in a disordered face-centered cubic γ matrix represent a new opportunity for high-temperature alloy development. The emergence of alloys with low density and high specific yield strength at elevated temperatures has further energized the research and development efforts in the last 5 years. Initially stabilized by the addition of small amounts of Nb and Ta, these new generations of alloys with multiple alloying additions to form basic quaternary and ternary alloys have steadily expanded the property envelopes to raise hope for a modern class of superalloys with higher-temperature capabilities. This article reviews the work of a vibrant set of researchers across the globe whose findings are constantly unlocking the potential of these alloys. These developments have achieved high-temperature strength (at 870°C) >0.6 GPa, γ' solvus temperature exceeding 1,100°C, and densities between 7.8 and 8.6 g/cm^3.

1. INTRODUCTION

The discovery of γ/γ′ microstructure with the addition of W to a Co-Al alloy has opened up new possibilities for high-temperature alloy development (1, 2). Like Ni-Al base superalloys, the strengthening of these alloys occurs by the coherent precipitation of $L1_2$ ordered γ′ precipitates with the stoichiometry $Co_3(Al,W)$ in a face-centered cubic (fcc) γ-Co matrix. However, the γ/γ′ lattice parameter mismatch is positive in these alloys (2, 3). Extensive efforts are being made to overcome some of the drawbacks related to the stability of the γ′ phase and high mass densities (>9.5 g/cm^3) using alloying additions like Ni, Ti, Ta, Mo, and Cr and have been reviewed extensively (2, 4–13).

The addition of W (19.3 g/cm^3), up to 25 wt%, played an essential role in the early development of γ/γ′ Co-Al-W superalloys, and it was thought that W was necessary for stabilizing the γ/γ′ microstructure. A shift in this thought occurred with a series of publications in 2015 that revealed stabilization of the γ/γ′ microstructure in the Co-Al-Mo system, without W addition, by a small amount of Nb or Ta (14–16). These alloys were labeled W-free Co base superalloys. Later, extensive development took place on the design of new, low-density γ/γ′ Co base alloy compositions with competitive high-temperature mechanical properties, γ′ phase stability, and oxidation resistance with mass densities in the range of 7.8–8.6 g/cm^3. This review summarizes these developments and sheds light on the way to unlock their potential in the domain of high-temperature alloys. We have divided the review into five sections: microstructure and physical properties of new γ/γ′ Co base superalloys, mechanical properties, oxidation properties, hot workability, and future prospects. To systematize the narratives, the alloys are classified in terms of their basic compositions. These are primarily the quaternary alloys of Co-Al-Mo-Nb/Ta (Q^{Co}_{Mo}), Co-Al-Cr-Nb/Ta (Q^{Co}_{Cr}), and Co-Al-V-Nb/Ta (Q^{Co}_{V}) and ternary alloys of Co-Al-Ta/V (T^{Co}_{Al}), Co-Ti-Cr/Mo/V (T^{Co}_{Ti}), and Co-V-Ta/Nb (T^{Co}_{V}).

2. MICROSTRUCTURE AND PHYSICAL PROPERTIES OF NEW γ/γ′ Co BASE SUPERALLOYS

2.1. Quaternary Base Alloys

This section briefly describes the properties of W-free Co base compositions exhibiting the γ/γ′ microstructure stabilized by Mo/Ta, Mo/Nb, and Ta/Cr in the Co-Al system.

2.1.1. Co-Al-Mo-Nb/Ta. In 2015, Makineni et al. (14) reported a Co base alloy with a γ-Co fcc matrix strengthened by $L1_2$ ordered γ′ precipitates without W addition (**Figure 1*a***). The alloy composition was Co-10Al-5Mo-2Nb [henceforth all in atomic percent (at%)] with a mass density of 8.36 g/cm^3, 1.2 g/cm^3 lower than that of the Co-8.8Al-9W base alloy. Atomic-scale compositional analysis reveals strong partitioning of Mo and Nb to γ′ with respect to γ, while Al partitions equally between γ′ and γ (**Figures 1*d*** and **2**). The strengthening γ′ phase exhibits a cuboidal morphology and crystalizes into a stoichiometric $Co_3(Al,Mo,Nb)$ intermetallic with an $L1_2$ ordered structure. The microstructure consists of γ′ precipitates (~40-nm size) homogeneously distributed with a γ′ volume fraction of ~54% when aged at 800°C for 2 h. However, the γ′ solvus was measured to be ~866°C, lower by ~124°C than the Co-8.8Al-9W superalloy. Additionally, upon aging at 800°C beyond 35 h, the γ/γ′ microstructure decomposes to the equilibrium phases fcc γ-Co (with a different composition from the original matrix), B2 ordered CoAl, and DO_{19} ordered $Co_3(Nb,Mo)$, indicating the metastable nature of the $L1_2$ $Co_3(Al,Mo,Nb)$ phase (17).

Yao et al. (20) performed first-principles calculations on the $L1_2$ $Co_3(Al,Mo,Nb)$ intermetallic phase with the composition Co-9.375Al-9.375Mo-6.25Nb to assess its phase stability as well as its elastic and thermodynamic properties. The electronic density of states and the Fermi level

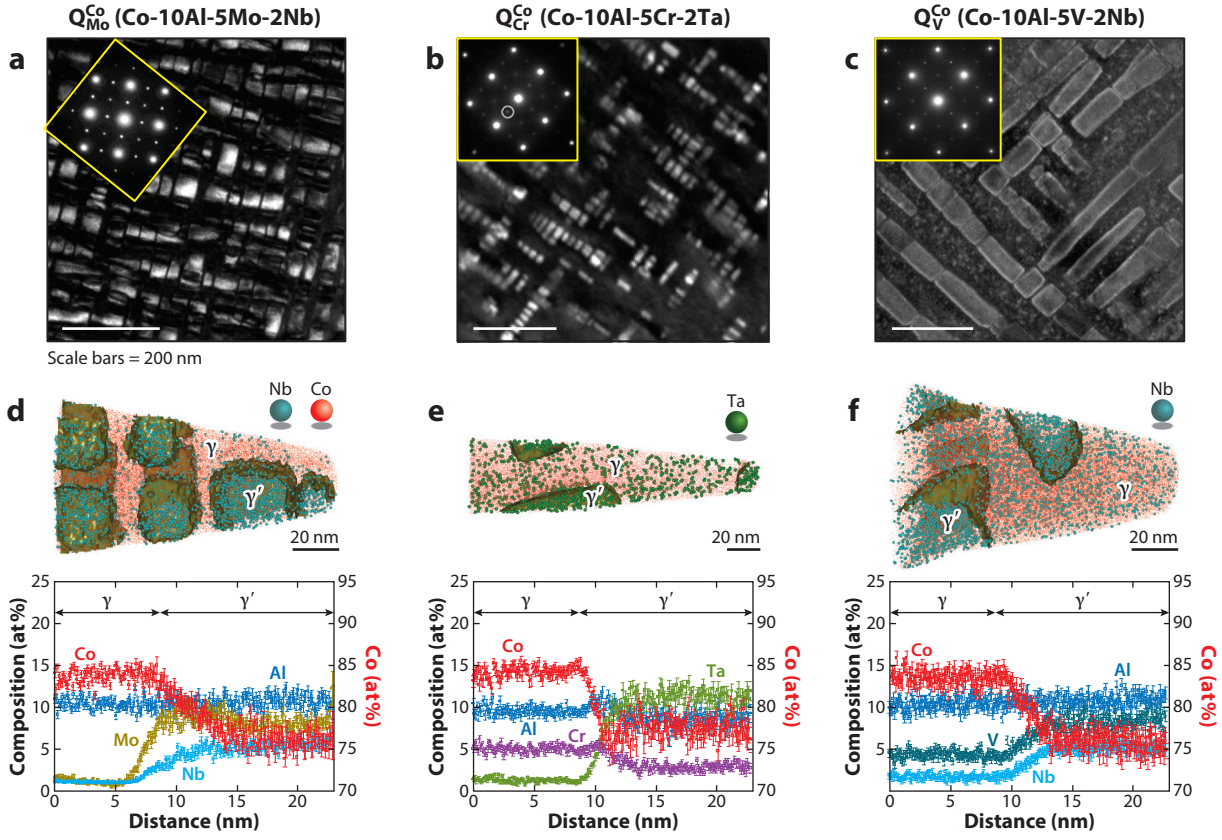

Figure 1

Transmission electron micrographs (dark-field images) for (*a*) Co-10Al-5Mo-2Nb (Q^{Co}_{Mo}), (*b*) Co-10Al-5Cr-2Ta (Q^{Co}_{Cr}), and (*c*) Co-10Al-5V-2Nb (Q^{Co}_{V}) alloys showing coherent cuboidal $L1_2$ γ′ precipitates with stoichiometry of Co_3(Al,Mo,Nb), Co_3(Al,Cr,Ta), and Co_3(Al,V,Nb), respectively. (*d–f*) Atom probe reconstructions and composition profiles across a γ/γ′ interface for the corresponding alloys (Co composition is on the right *y*-axis scale in each plot). The alloys were homogenized at 1,200°C for 20 h, followed by aging at 800°C for 2 h for the Co-10Al-5Mo-2Nb and Co-10Al-5Cr-2Ta alloys and 10 h for the Co-10Al-5V-2Nb alloy. Panel *a* adapted with permission from Reference 14, panel *b* adapted with permission from Reference 18, and panel *f* adapted with permission from Reference 19.

for the phase fall in the bonding states, indicating that the Co_3(Al,Mo,Nb) phase is stable. The shear and Young's moduli for Co_3(Al,Mo,Nb) are larger than those of Ni_3Al and smaller than those of the Co_3(Al,W) phase with the composition Co-12.5Al-12.5W. The elastic anisotropy parameter *A* of Co_3(Al,Mo,Nb) is smaller than that of Co_3(Al,W) and Ni_3Al. The *B*/*G* ratio and Cauchy pressure ($C_{12}-C_{44}$) were >1.75 and positive for Co_3(Al,Mo,Nb), suggesting its ductile nature compared to Co_3(Al,W). The Young's modulus for Co_3(Al,Mo,Nb) along the <111> direction (E_{111}) is larger by 200 GPa than that along <100> (E_{100}). This difference is similar to that reported for Co_3(Al,W) and Ni_3Al phases (**Table 1**). Yao et al. (20) also found that the thermodynamic properties, such as entropy and coefficient of thermal expansion of Co_3(Al,Mo,Nb), exhibit temperature-dependent behavior. At the same time, the formation enthalpy remains constant with an increase in temperature.

The replacement of Nb by Ta further stabilizes the γ′ phase (15). The polycrystalline alloy Co-10Al-5Mo-2Ta upon aging at 800°C for 10 h yields a homogeneous distribution of γ′ cuboidal

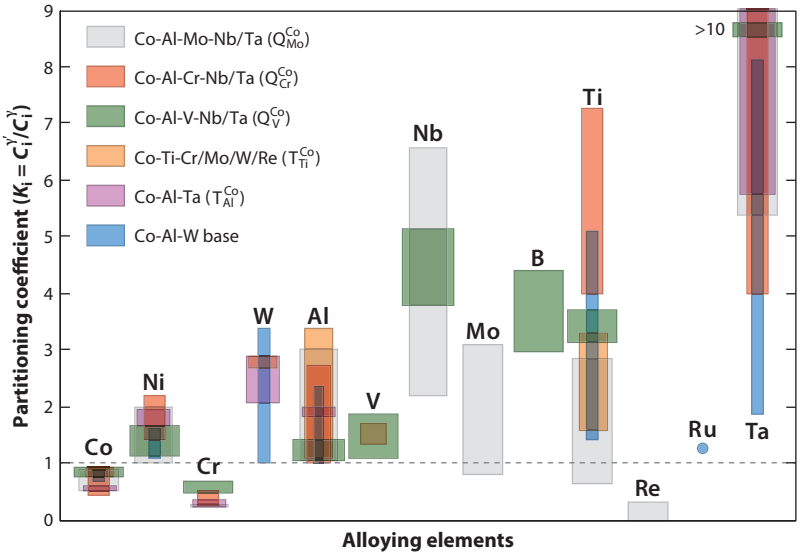

Figure 2

Comparison of elemental partitioning of solutes in low-density quaternary (Q^{Co}), ternary (T^{Co}), and Co-Al-W base superalloys. Data from References 14–16, 18, 22–24, 29–31, 37–43, and 44; P. Pandey, N. Majumdar, M.P. Singh, C. Patil, A. Sharma, et al., unpublished manuscript.

precipitates (58% volume fraction) in the γ matrix. The γ′ solvus also increased by 62°C to 928°C relative to the Co-10Al-5Mo-2Nb alloy. Atomic-scale compositional analysis reveals strong partitioning of Ta into γ′, which also induces an increase in the Al partitioning to γ′ (**Figure 2**) (15). The measured γ′ composition Co-12.9Al-5.9Mo-3.7Ta supports the stoichiometry as Co_3(Al,Mo,Ta). Interestingly, Feng et al. (5) came close to a W-free Co base superalloy with Ta stabilization. However, their composition contained 9 at% Mo, which results in the coexistence of needles of a Co_3Mo intermetallic compound along with γ′ precipitates.

The increase in γ′ stability by Ta partitioning is due to the enhanced *d-d* hybridization among the transition metals in the $L1_2$ Co_3(Al,Mo,Ta) intermetallic; hence, the formation enthalpy (ΔH_f) for the $L1_2$ structure becomes more negative compared to the DO_{19} structure (15). Omori et al. (22) illustrated that the solutes with stronger partitioning to γ′ have more negative formation enthalpies that also directly correlate with the increase in γ′ solvus temperature. For example, Co_3Ta in the $L1_2$ structure has a more negative formation enthalpy than Co_3Al, Co_3Mo, or Co_3Nb;

Table 1 Calculated single-crystal and polycrystalline elastic constants, including C_{ij}, B_b, G_b, E_b, B/G, Cauchy pressure $C_{12}-C_{44}$, and elastic anisotropy parameters A, for Co_3(Al,Mo,Nb) at 0 K in comparison with Co_3(Al,W) and Ni_3Al

Intermetallic compound	Single-crystal elastic constants (GPa)			Polycrystalline elastic constants (GPa)			Elastic anisotropy parameters					
	C_{11}	C_{12}	C_{44}	B_b	G_b	E_b	A	E_{111}	E_{100}	$\frac{E_{111}}{E_{100}}$	$C_{12}-C_{44}$	$\frac{B_b}{G_b}$
Co_3(Al,Mo,Nb)	290.7	176.6	149.6	214.6	101.7	263.4	2.62	364.2	157.2	2.32	27.0	2.11
Co_3(Al,W)	304.1	184.6	175.9	224.4	114.2	292.9	2.94	302.2	104.9	2.54	8.7	1.96
Ni_3Al	226.9	143.5	123.1	171.3	79.8	207.3	2.95	297.9	115.7	2.57	20.4	2.15

B_b, G_b, and E_b are the calculated bulk, shear, and Young's moduli of the compounds. Data from References 20 and 21.

hence, Ta can strongly partition to γ′ and increase the γ′ solvus temperature. This can also directly affect the γ′ volume fraction, as an increase in the solvus temperature leads to a steeper solvus line in the phase diagram. This decreases the solute solubility limit of the solute in the γ matrix, and a higher volume fraction of γ′ can be obtained during aging. Hence, the γ′ volume fraction increases by 4% in the Co-10Al-5Mo-2Ta alloy due to an increase in the γ′ solvus compared to the Co-10Al-5Mo-2Nb alloy. This direct correlation constitutes a basic guideline for alloying element selection in new Co base compositions for improving the γ/γ′ stability at high temperatures.

2.1.2. Co-Al-Cr-Nb/Ta. Pandey et al. (18) reported the stabilization of an $L1_2$ phase in a Co-Al-Cr base alloy by the addition of 2 at% Ta. The alloy Co-10Al-5Cr-2Ta, after solutionizing (1,200°C) and aging (800°C), yielded cuboidal $L1_2$ γ′ precipitates homogeneously distributed in the fcc γ-Co matrix (**Figure 1*b***). The alloy density is 8.43 g/cm^3, ∼1.1 g/cm^3 lower than that of Co-8.8Al-9W. Compositional analysis across γ/γ′ interfaces indicates Ta strongly partitions to γ′ with a partition coefficient $K_{Ta} > 10$, while Co and Cr partition preferably to the γ matrix (**Figures 1*e*** and **2**). However, Al shows no preferential partitioning, $K_{Al} \sim 1$, as was also observed in Co-8.8Al-9W and Co-10-Al-5Mo-2Nb alloys. The measured composition of γ′ indicates its stoichiometry to be Co_3(Al,Cr,Ta). The γ′ solvus temperature for the alloy was measured to be ∼870°C.

2.1.3. Co-Al-V-Nb/Ta. Recent work by Singh et al. (19) showed that replacement of Mo with the lighter V in the Co-10Al-5Mo-2Nb alloy could also result in a homogenous distribution of γ/γ′ precipitates (**Figure 1*c***). The γ′ volume fraction and γ′ solvus increase up to 58% and 876°C, respectively, and the mass density reduces to 8.12 g/cm^3. Compositional analysis across the γ/γ′ interface reveals a strong partitioning of V along with Nb to γ′, while Al equally partitions across γ and γ′ (**Figures 1*f*** and **2**). The γ′ composition indicates its stoichiometry to be Co_3(Al,V,Nb). Like the Co-10Al-5Mo-2Nb alloy, the V-containing alloy decomposes to equilibrium phases B2-Co(Al,V) + DO_{19}-Co_3Nb + γ-Co upon aging at 800°C for 200 h (19).

2.2. Ternary Alloys

Lee (1), in addition to work on Co-Al-W alloys, also reported $L1_2$ precipitates in ternary Co-Al-Nb and Co-Al-Ta systems. However, it is only recently that these alloys and a few other ternary systems have been explored.

2.2.1. Co-Al-V/Ta. Chen et al. (23) reported a γ/γ′ two-phase region in a ternary Co-Al-V system with a γ′ phase field broader than that observed in Co-Al-W. The microstructure in a Co-5Al-14V alloy after aging at 900°C for 48 h reveals γ′ precipitates with a round-cornered cuboidal shape and a γ′ volume fraction of ∼60%. The compositional analysis shows that both V and Al preferentially partition to γ′, stabilizing the $L1_2$ structure. The γ′ solvus temperature and mass density are measured to be ∼964°C and ∼8.11 g/cm^3, respectively. The γ/γ′ microstructure was stable even after exposure for 4,000 h at 900°C.

Recently, Chen et al. (24) also reported the formation of the metastable cuboidal γ′ Co_3(Al,Ta) phase with an $L1_2$ structure embedded in the γ-Co matrix in a Co-12Al-2Ta alloy when aged at 800°C for 48 h. This phase was earlier reported by Lee (1) in an alloy with a similar composition. The compositional analysis reveals a strong partitioning of both Ta and Al to γ′. The mass density of the alloy was found to be 8.33 g/cm^3, while the γ′ solvus was 949°C, higher than those of the quaternary Co-Al-Mo-Nb/Ta and Co-Al-Cr-Ta alloys. However, the stability of γ′ is relatively

lower: After exposure for 168 h at 800°C, the γ/γ′ microstructure decomposes to equilibrium phase mixtures of γ-Co + B2-CoAl + χ-Co_7Ta_2.

2.2.2. Co-Ti-Cr/Mo/V/W. As in the Ni-Al phase diagram, a stable γ′ Co_3Ti phase with $L1_2$ structure exists in the binary Co-Ti phase diagram (25). Alloys strengthened by these γ′ precipitates were not pursued earlier due to the low γ′ volume fraction of ∼20% at 900°C and high γ/γ′ lattice misfit (0.75–1.36%) as well as the presence of a discontinuous mode of the γ′ precipitation leading to poor high-temperature properties (26–28). The Co_3Ti intermetallic phase also has a lower solubility of other alloying elements. Except for Fe and Cr, most of the alloying elements, upon aging, destabilize the $L1_2$ phase and promote the formation of phases, such as Ni_3Ti (DO_{24}), β-Co_3W (DO_{19}), or Laves phases (28). However, the alloy Co-10.7Ti-11Cr yields a γ/γ′ microstructure that remains stable up to 1,000 h at 1,000°C (28). Zenk et al. (29) have shown that the Co-11Ti-15Cr alloy, solutionized (1,150°C) and aged at 900°C for 100 h, exhibits coherent cuboidal γ′ precipitates with a volume fraction of 66% and a γ/γ′ misfit of 0.54%. Cr inhibits the γ′ cellular precipitation, unlike in the case of binary Co-Ti alloys. The spatial distribution maps by atom probe tomography of Co-12Ti-4Cr reveal that Cr prefers partitioning to the γ matrix and Ti to γ′. The γ′ stoichiometry was identified as Co_3(Ti,Cr) with Cr sharing the Ti sublattice sites (30). The presence of Cr partially releases Ti, and due to the presence of these excess Ti atoms, the γ′ volume fraction increases to ∼52% in the ternary alloy from ∼ 41% in the binary Co-12Ti alloy as excess Ti promotes γ′ formation (30).

The γ′ precipitates in the binary Co-12Ti alloy were plate/rod shaped due to a high γ/γ′ lattice misfit of ∼1.2% (30). Addition of 4 at% Mo to the Co-12Ti alloy changes the γ′ morphology to cuboidal when aged at 800°C, with a reduced misfit of 1% (30, 31). Mo also increases the γ′ volume fraction to 65% and γ′ solvus to 1,119°C (versus 1,005°C for the binary alloy). The experimentally determined γ′ stoichiometry is Co_3(Ti,Mo). The ternary phase equilibria of Co-Ti-V between 800°C and 1,000°C has been recently reported by Ruan et al. (32). For Co-5Ti-15V, the volume fraction of γ′ precipitates at 800°C is ∼79% with a γ′ solvus of 1,091°C. Here, both Ti and V strongly partition to γ′. Yoo et al. (33) demonstrated the formation of cuboidal γ′ precipitates in Co-15Ti-3W with a volume fraction of ∼66% upon aging at 900°C for 48 h. The γ/γ′ lattice misfit was reduced to ∼0.69%, and the γ′ solvus increased to 1,144°C. The compositional analysis shows W partitions to γ′ along with the Ti, which explains the stabilization of the γ/γ′ microstructure at higher temperatures with the addition of W to Co-Ti.

2.2.3. Co-V-Ta/Nb. Nyshadham et al. (34) recently reported first-principles calculations to search for new alloy systems that can form stable $L1_2$ precipitates by computing formation enthalpy and decomposition energy values. They identified two Co base systems, Co-V-Ta and Co-V-Nb, that might form a γ/γ′ microstructure with Co_3(V,Ta) and Co_3(V,Nb) $L1_2$ precipitates in the γ-Co matrix. These two stoichiometries show lower decomposition energies (19 and 18 meV/atom, respectively) and more negative formation enthalpy values (−156 and −189 meV, respectively) compared to Co_3(Al,W), which has the values 66 meV/atom and −130 meV, respectively. In line with this expectation, Reyes Tirado et al. (35) experimentally established the formation of the γ/γ′ microstructure in Co-6V-6Ta and Co-6V-6Nb alloys after solutionizing at 1,250°C and aging at 900°C. Upon aging, the alloys exhibit cuboidal γ′ precipitates in the γ matrix in addition to coarser C36 Laves phases in Co-6V-6Ta and needle-like precipitates of DO_{19} in the Co-6V-6Nb alloy. Compositional analysis reveals that Ta and Nb strongly partition to γ′, while V partitions weakly to γ′. Recently, Ruan et al. (36) used machine learning and CALPHAD (calculation of phase diagrams) methods to identify the composition of Co-12V-2Ta with a solvus

of 974°C and a density of 8.86 g/cm^3. This alloy exhibited a γ/γ′ microstructure (~31% volume fraction of γ′) at 800°C without the presence of any additional phases.

The degree of elemental partitioning of solutes is compared for the quaternary and ternary classes of alloys in **Figure 2**.

2.3. Alloying Effects

The alloying additions and their partitioning across γ and γ′ play critical roles in tuning the microstructure, γ′ volume fraction, γ′ solvus temperature, and γ/γ′ lattice misfit that in turn control the γ′ stability, γ′ coarsening behavior, and mechanical properties of these alloys at high temperatures.

2.3.1. Ni addition. The addition of Ni and its synergy with other alloying additions increase the γ′ phase field of these low-mass-density Co base alloys similar to that reported for Co-Al-W base alloys (45). In Q^{Co}_{Mo}, substitution of 30 at% Ni for Co in Co-10Al-5Mo-2Nb increases the solvus by 124°C (to 990°C) and the γ′ volume fraction to 76% upon aging at 800°C. Ni strongly partitions to γ′, replacing Co, and enhances the partitioning of Al to γ′. Compositional analysis establishes the γ′ stoichiometry to be $(Co,Ni)_3(Al,Mo,Nb)$. The γ/γ′ lattice misfit was estimated to be ~0.32 (20, 36). The increase in Al partitioning to γ′ might be due to the strong affinity of Al atoms toward Ni in an $L1_2$ unit cell since the stability of Ni_3Al is higher than that of Co_3Al. Similarly, in Co-10Al-5Mo-2Ta, the γ′ volume fraction increases to 74% with 30% Ni substitution when aged at 800°C, while the γ′ solvus increases to 1,014°C, higher than that for the Co-8.8Al-9W superalloy (15). First-principles calculations reveal that Ni occupancy at Co sites in $L1_2$ shifts the Fermi level toward the pseudogap, which increases the negative value of the formation enthalpy and, thus, the structural stability of the $L1_2$ phase (15). Since the mass density of Ni is close to that of Co, the alloy densities remain similar to the base compositions.

In T^{Co}_{Al} alloys, the effect of Ni is more prominent. For example, in the Co-12Al-2Ta alloy, with an increase of Ta to 8 at% and substitution of 30 at% Ni, the γ′ solvus increases by 238°C, reaching a value of 1,286°C (24). The mass density of the alloy also increases to 9.21 g/cm^3 due to the higher density of Ta (16.6 g/cm^3). At 4 at% Ta, the mass density reduces to 8.64 g/cm^3 with simultaneous reduction of the γ′ solvus to 1,161°C. In general, the addition of 30 at% Ni is standard in most of the currently developed Co base superalloys.

2.3.2. Ti addition. Among the solutes, Ti is the most effective at increasing the γ′ volume fraction and γ′ solvus temperature in Co alloys. The addition of 4 at% Ti to the Co-30Ni-10Al-5Mo-2Ta alloy (Q^{Co}_{Mo}) resulted in an increase in the γ′ solvus temperature to 1,166°C, while the γ′ volume fraction increases to 83% (compared to 50% for the alloy without Ti) upon aging at 900°C (37). In the Co-30Ni-10Al-5Cr-2Ta alloy (Q^{Co}_{Cr} class), a similar addition (4 at% Ti) increases the γ′ volume fraction and solvus temperature to 63% and 1,128°C, respectively, while the lattice misfit reduces from 0.99 to 0.71 (18). Ti partitions to γ′, imparting additional stability to the γ′ phase. Ti addition also suppresses the directional coarsening and coagulation of γ′ precipitates after long exposure at high temperatures (18). The tendency of alloys like Co-30Ni-10Al-5Mo-2Nb to form topologically close-packed (TCP) phases when exposed to high temperatures (>900°C) can be suppressed with the addition of 2 at% Ti (41). In Co-12V-2Ta (T^{Co}_{V}) (32), an equilibrium Co_3V phase forms intergranularly during long-term (~720 h) aging at 800°C. The addition of 2 at% Ti suppresses the formation of this phase and increases the γ′ solvus to 1,044°C (from 974°C). The resultant mass density decreases to 8.71 g/cm^3 (from 8.86 g/cm^3). An optimized composition of

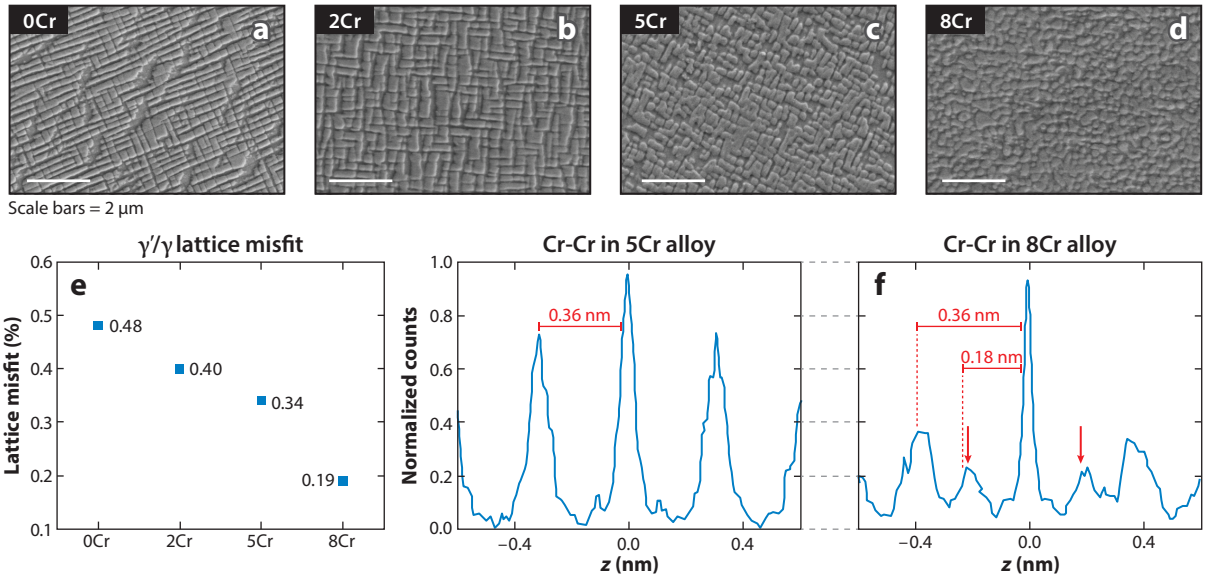

Figure 3

Secondary electron micrographs for Co-30Ni-10Al-5Mo-2Ta-2Ti (Q^{Co}_{Mo}) with (*a*) 0Cr, (*b*) 2Cr, (*c*) 5Cr, and (*d*) 8Cr. The alloys were homogenized at 1,250°C for 25 h, followed by aging at 900°C for 50 h, and show transition of the γ′ morphology from sharp-edge cuboidal to round-cornered cuboidal to spherical. (*e*) A plot showing a decrease in the γ/γ′ lattice misfit as Cr increases. (*f*) Spatial distribution maps from successive {100} planes for γ′ in 5Cr and 8Cr alloys along the [100] direction, indicating that Cr also occupies {1/2,1/2,0} site positions in the 8Cr alloy (*red arrows*). Figure adapted with permission from Reference 40.

Co-30Ni-10Al-5V-4Ta-2Ti (T^{Co}_{V}) has been reported that exhibits a combination of high γ′ solvus (1,243°C) and low mass density (8.46 g/cm^3) (23).

2.3.3. Cr addition. Cr plays a crucial role in imparting resistance to high-temperature oxidation and corrosion in superalloys. However, the addition of Cr also regulates the γ/γ′ lattice misfit and, hence, the γ′ morphology. Pandey et al. (40) reported a reduction of the lattice misfit from 0.48 to 0.19 with the addition of Cr up to 8 at% in a Co-30Ni-10Al-5Mo-2Ta-2Ti alloy (Q^{Co}_{Mo}). Cr also induces a morphological transition of γ′ in the sequence of cuboidal to round-cornered cuboidal to spherical (**Figure 3*a–e***). The reduction in lattice misfit is due to three factors: (*a*) strong partitioning of larger Cr atoms to the γ matrix, (*b*) Cr preference for B sites in the A_3B $L1_2$ lattice, and (*c*) inversion of partition behavior of the larger Mo atoms from γ′ to γ with Cr addition. These conclusions were supported experimentally by generating elemental spatial distribution maps along the [001] cubic axis with atom probe tomography (**Figure 3*f***) and first-principles calculations. The lowering of the γ/γ′ lattice misfit reduces the strain energy contribution to the total free energy. Hence, the domination of the interfacial energy leads to the transition to spherical γ′ precipitate morphology. A similar reduction in the γ/γ′ lattice misfit and a change in the γ′ morphology due to Cr addition was also observed in Co-30Ni-12Al-4Ta (T^{Co}_{Al}) and Co-15Ti-3W (T^{Co}_{Ti}) alloys (24, 33). Cr, up to a critical amount, was also shown to increase the γ′ solvus and γ′ volume fraction. However, the degree of increment differs depending on the alloy class. Additionally, Cr reduces the alloy mass density by ∼0.02 g/cm^3 per at% of Cr.

2.3.4. Re addition. Re has a significant effect by enhancing the high-temperature mechanical properties in Ni base superalloys. Some studies have indicated that Re did not improve the creep

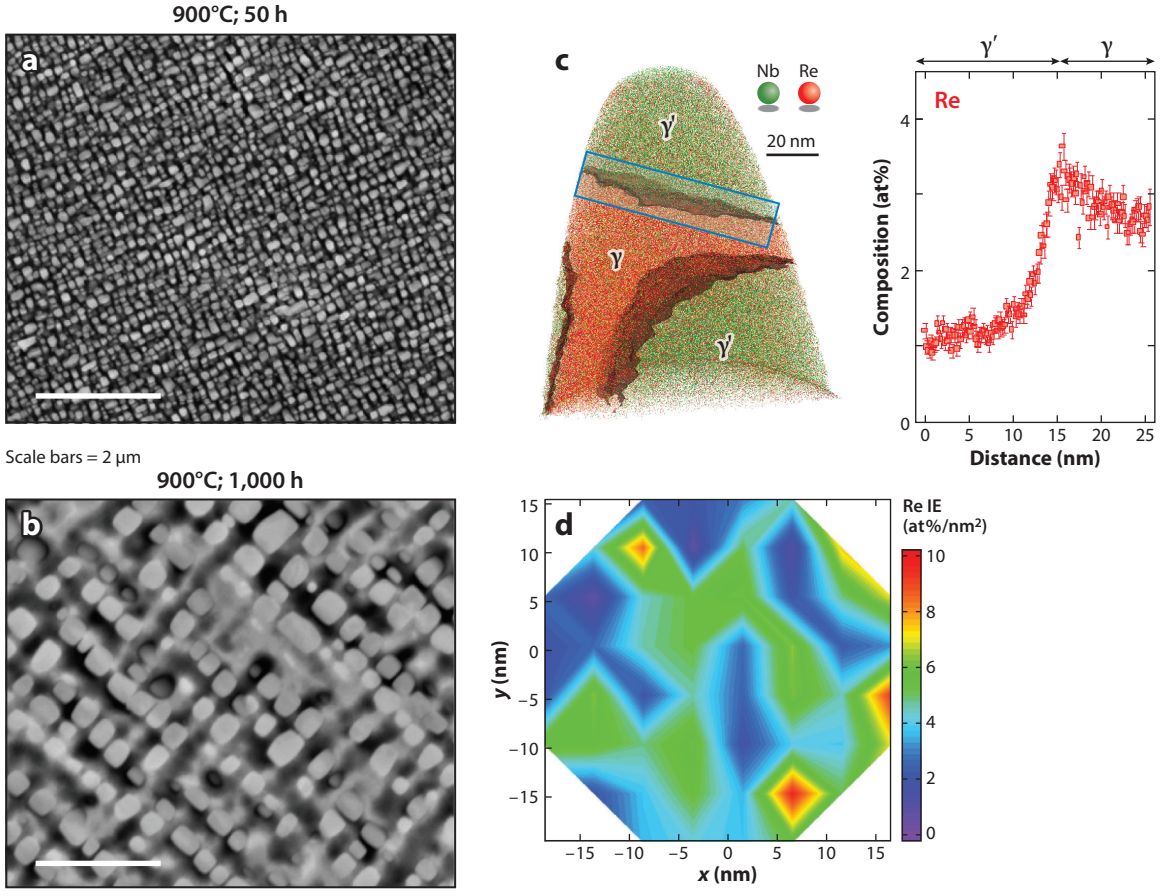

Figure 4

(*a*,*b*) Backscattered secondary electron micrographs for the Co-30Ni-10Al-5Mo-2Nb-2Re (Q_{Mo}^{Co}) alloy showing γ′ precipitates in the γ matrix after solutionizing at 1,250°C for 20 h, followed by aging at 900°C for (*a*) 50 h and (*b*) 1,000 h. (*c*) An atom probe reconstruction of a needle specimen from the alloy indicating the distribution of Nb (*green*) and Re (*red*) atoms across the γ/γ′ interface and composition profile of Re across the interface (*blue rectangle*), showing evidence of significant interfacial segregation. (*d*) 2D quantitative maps showing the variations of Gibbsian interfacial excess (IE) of Re along the γ/γ′ interface marked by the semitransparent cube in the atom probe reconstruction. Figure adapted with permission from Reference 38.

properties of Co-Al-W base alloys due to lower partitioning of Re to the γ matrix (46, 47). Although Re has a minor influence on the solvus temperature and increases the density, Pandey et al. (38) showed that 2 at% Re addition to the Co-30Ni-10Al-5Mo-2Nb alloy (Q_{Mo}^{Co}) does influence the coarsening of γ′ precipitates due to a reduction of the γ/γ′ lattice misfit up to 40% (from 0.32 to 0.19) that also induces rounding of the γ′ precipitate shape (**Figure 4*a***). In contrast to Co-Al-W base alloys, Re strongly partitions to the γ matrix in Q_{Mo}^{Co} alloys and segregates at the γ/γ′ interface (**Figure 4*c*,*d***). It also enhances the partitioning of larger Mo atoms to γ. The low γ/γ′ misfit and Re segregation reduce the interfacial energy and lower the γ′ coarsening rate at 900°C, stabilizing the γ/γ′ microstructure even after 1,000 h of exposure (**Figure 4*b***) with minimal effect on volume fraction. Without Re, the γ′ volume fraction decreases rapidly in the Co-30Ni-10Al-5Mo-2Nb alloy after 100 h of exposure at 900°C (48).

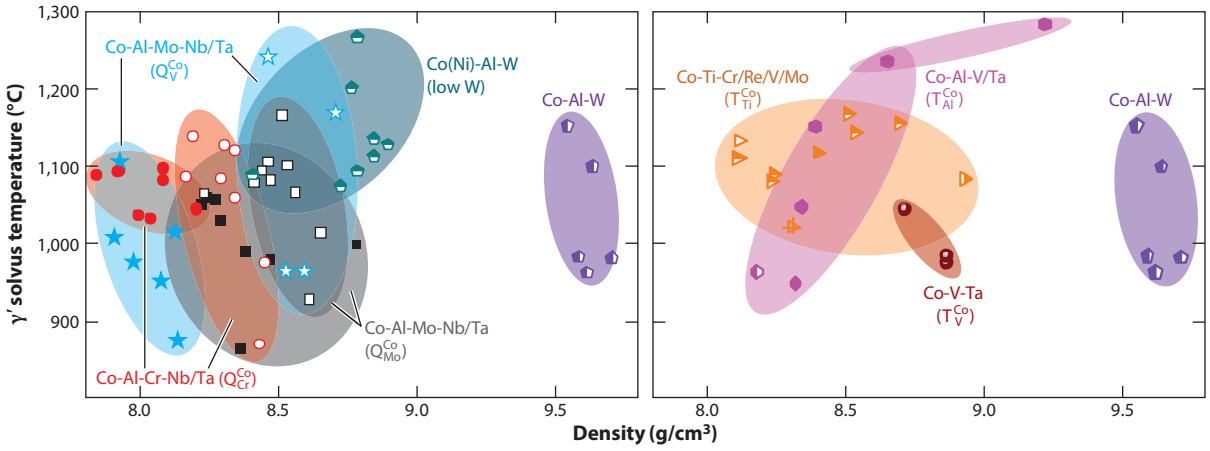

Figure 5

Ashby plots between the γ′ solvus and density for the quaternary (Q^{Co}) and ternary (T^{Co}) alloys compared to high W– and low W–containing Co-Al-W base superalloys. Data reported from References 11, 14–16, 18, 19, 23, 24, 30, 36, 37–42, and 48–51.

Li et al. (42) studied the influence of Re addition (up to 5 at%) on the Co-12Ti (T_{Ti}^{Co}) alloy. The solvus increases from 1,022°C for the binary alloy to 1,085°C, with a precipitate volume fraction of 53%, for the Re-added alloy. Re also reduces the γ/γ′ lattice misfit to 0.5% and reduces the coarsening of γ′ precipitates while increasing density to 8.92 g/cm^3.

The quaternary (Q^{Co}) and ternary (T^{Co}) alloys were further developed through alloying additions to yield higher γ′ solvus temperature and lower mass density values. **Figure 5** shows Ashby plots between the γ′ solvus and density for both the Q^{Co} and T^{Co} alloys compared to high W–containing Co-Al-W base and low W–containing Co(Ni)-Al-W base superalloys. The plots indicate that Ta-containing alloys have a higher γ′ solvus than Nb-containing alloys in all the outlined classes. Among these, some of the Ta-containing Q_{Mo}^{Co} and Q_V^{Co} alloys have γ′ solvus temperatures greater than 1,100°C with densities in the range of 8.5 to 8.7 g/cm^3 compared to high W–containing Co-Al-W base alloys having lower γ′ solvuses and higher densities. While some of the low W–containing Co(Ni)-Al-W base alloys show γ′ solvuses up to 1,250°C, their densities are still >8.8 g/cm^3. Some of the Ta-containing Co-Al base superalloys (T_{Al}^{Co}) show a promising combination of high γ′ solvus temperatures (>1,100°C) and moderate density values. In summary, the plots reveal a developmental trend in the design of low-density superalloys.

2.3.5. γ′ coarsening behavior. Few reports exist on the effect of alloying on the coarsening behavior of γ′ precipitates in low-density Co base alloys. A summary of the available data of γ′ coarsening rate constants (K_r) of these alloys obtained at 800°C and 900°C is shown in **Figure 6**. Here, the K_r is directly proportional to the γ/γ′ interface energy σ and diffusion coefficient D of the slowest diffusing species in the matrix. The coarsening kinetics are slower when these two terms are lower (52).

In the Co-30Ni-10Al-5Mo-2Nb (Q_{Mo}^{Co}) alloy, γ′ precipitates show accelerated directional coarsening by coalescence and coagulation along <100> at 900°C, with an increase in mean width of γ′ from 220 ± 70 nm after 50 h to a mean width and length of 600 ± 130 nm and 1,400 ± 110 nm, respectively, after 1,000 h of aging (48). Additionally, the γ′ volume fraction drops from 50% after 50 h to 35% after 200 h to 25% after 1,000 h of aging. Similar directional coarsening and dissolution of γ′ is observed in Co-Al-W base and Ni-Al base alloys upon long-term aging at

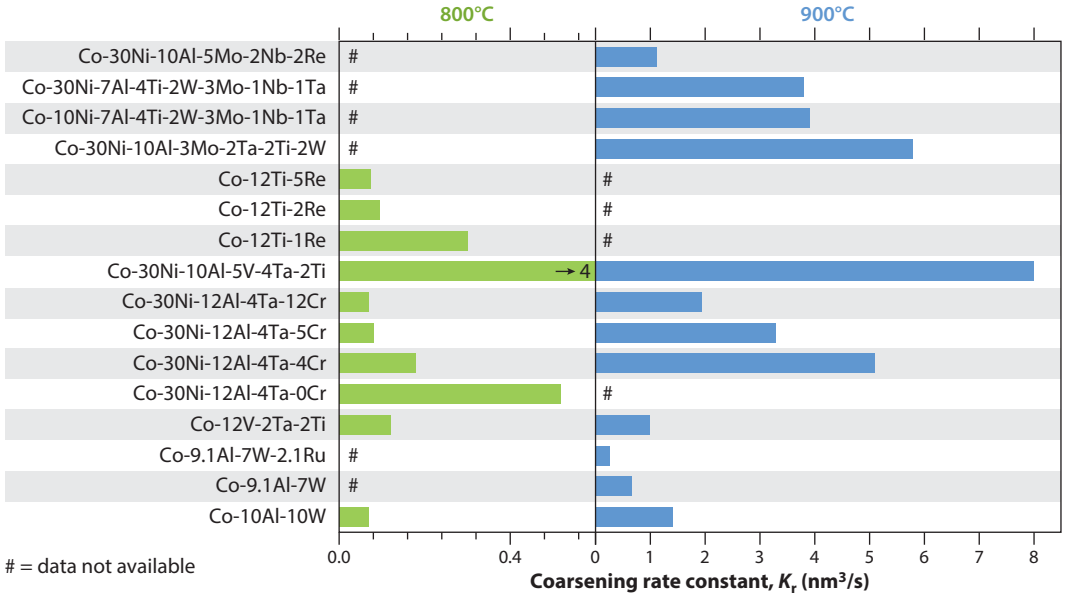

Figure 6

Comparison of the γ′ coarsening rate constant (K_r) for several low-density Co base superalloys with Co-Al-W base superalloys at 800°C and 900°C. Data obtained from References 23, 24, 36, 38, 42, and 53–57.

temperatures near the γ′ solvus (58–62). Upon the addition of 2 at% Ti to Co-30Ni-10Al-5Mo-2Nb, directional coarsening of γ′ was not observed. The γ′ volume fraction increases to 58% after 50 h of aging at 900°C and remains unchanged up to 750 h, indicating that the alloys are in the coarsening regime. The estimated K_r value was 18.2 nm³/s for the alloy. In the Ta-stabilized alloy, Co-30Ni-10Al-5Mo-2Ta-2Ti, the K_r was lower, 3.8 nm³/s, at 900°C (37). The addition of 2 at% Re to the Co-30Ni-10Al-5Mo-2Nb alloy reduces K_r to 1.13 nm³/s, which is comparable to that observed in Co-Al-W alloys (38). Re also retards the γ′ coarsening kinetics in the Co-12Ti (T^{Co}_{Ti}) alloy. K_r decreases from 0.3 to 0.073 nm³/s with an increase in Re from 1 to 5 at% during aging at 800°C (42).

Addition of Cr up to 12 at% in Co-30Ni-12Al-4Ta (T^{Co}_{Al}) significantly enhances the γ′ coarsening resistance (24). K_r reduces from 0.5 to 0.07 nm³/s at 800°C due to the low misfit and low diffusivity of Cr. The coarsening resistance is comparable to that of the Co-10Al-10W alloy. Similarly, in the Co-12V-2Ta-2Ti (T^{Co}_{V}) alloy (63), the reported K_r values were 0.12 nm³/s and 1 nm³/s at 800°C and 900°C, respectively, comparable to the Co-10Al-10W alloy. Here, the slow coarsening kinetics were attributed to the presence of V as a solute, as it has a slower diffusion coefficient compared to Ta and Ti and thus is the rate-limiting element for γ′ coarsening in the alloy.

3. MECHANICAL PROPERTIES

3.1. Yield Strength

Figure 7 summarizes the temperature dependence of 0.2% yield strength (YS) as a function of temperature for the quaternary (Q^{Co}) and ternary (T^{Co}) alloys. The variation depends on the alloy compositions and often shows a yield stress anomaly (YSA) at higher temperatures. Similar behavior is also observed in Co-Ti binary (64, 65), Co-Al-W base (66, 67), and most Ni base

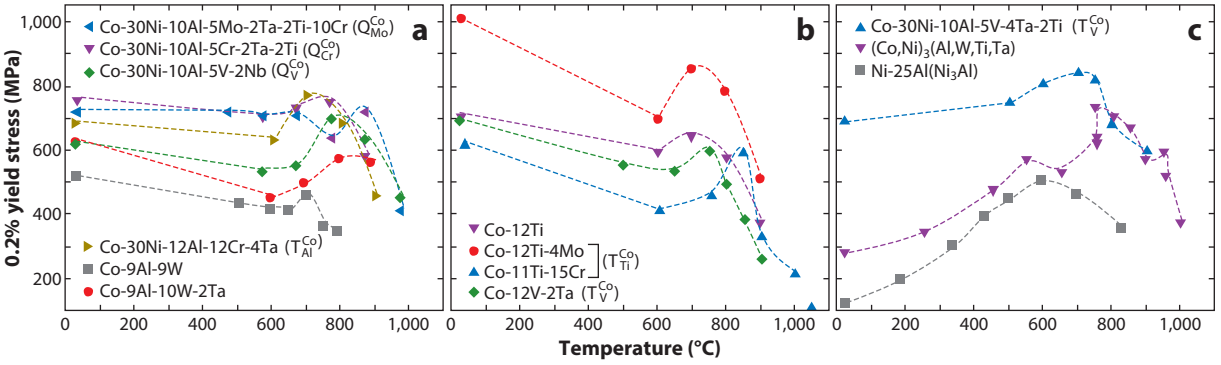

Figure 7

Comparison of 0.2% yield stress behavior as a function of temperature for (*a*) quaternary (Q^{Co}) and (*b*) ternary (T^{Co}) alloys and (*c*) Co-Al-W base alloys. Data from References 15, 16, 18, 19, 23, 24, 29, 31, 36, 37, 39, 67, and 71.

superalloys (68) that are strengthened by γ′ precipitates with $L1_2$ ordered structure. For the Co-30Ni-10Al-5Mo-2Ta-2Ti (Q^{Co}_{Mo}) alloy (15), the 0.2% YS decreases slightly up to 770°C and rapidly at higher temperatures (not shown in **Figure 7**). Upon further addition of 10 at% Cr to the alloy (39), the yield stress maintains a value of ~720 MPa to 670°C, followed by a drop to 650 MPa at 770°C before anomalously increasing to a peak value of 720 MPa at 870°C. Beyond this, the yield stress decreases rapidly (**Figure 7*a***). This phenomenon of initial decrease of 0.2% YS at low temperatures and its anomalous increase at higher temperatures was also observed in other Cr-containing alloys, like Co-30Ni-12Al-4Ta-12Cr (T^{Co}_{Al}) (24) and Co-30Ni-10Al-2Ta-4Ti-5Cr (Q^{Co}_{Cr}) (18). In Co-Al-W base alloys, a similar initial decrease in 0.2% YS was also observed and was attributed to a thermal component of solid-solution hardening in γ′ $Co_3(Al,W)$ during the motion of antiphase boundary (APB)-coupled dislocations (1/2<110> pairs). These APB pairs have a planar and glissile core structure that overcomes strain fields due to the large atomic size mismatch of elements in the $L1_2$ unit cell (69, 70).

For the Co-12V-2Ta base (T^{Co}_{V}) alloys, the 0.2% YS decreases more sharply with an increase in temperature to a minimum at 650°C before anomalously increasing with a peak at 750°C (36). A rapid decrease at higher temperatures follows this trend (**Figure 7*b***). A similar trend is also observed in Co-12Ti (31), Co-11Ti-15Cr (29), and Co-12Ti-4Mo (31) (T^{Co}_{Ti}) alloys. The initial rapid decrease of yield stress at low temperatures in Co_3Ti was ascribed to the thermally activated glide of partial dislocations ($b = 1/3<112>$) bound by a superlattice intrinsic stacking fault. The partials core is believed to be nonplanar and hence subject to lattice friction (72).

After a critical onset temperature, most of the alloys show an abrupt increase of 0.2% YS; Co-Ti base and Co-Al-W base alloys have been reported to reach a peak value. This anomalous increase might be attributed to the thermally activated cross-slip of APB-coupled dislocations from {111} planes to {010} planes in γ′, similar to that reported for Ni_3Al-strengthened Ni base superalloys (73). The 0.2% YS, in Ni_3Al, anomalously increases from low temperature (77 K). The cross-slip event leads to the locking of screw segments of the two partials coupled with an APB on the {010} plane. This locked configuration is popularly known as a Kear-Wilsdorf lock (73). The reason for a higher onset temperature for the anomalous increase in 0.2% YS in Co base alloys may be related to a higher activation energy for cross-slip, as reported in the case of $Co_3(Al,W)$ (69). The lower complex stacking fault (CSF) energy in $Co_3(Al,W)$ provides resistance to cross-slip of APB-coupled dislocations from {111} to {010} planes due to the formation of

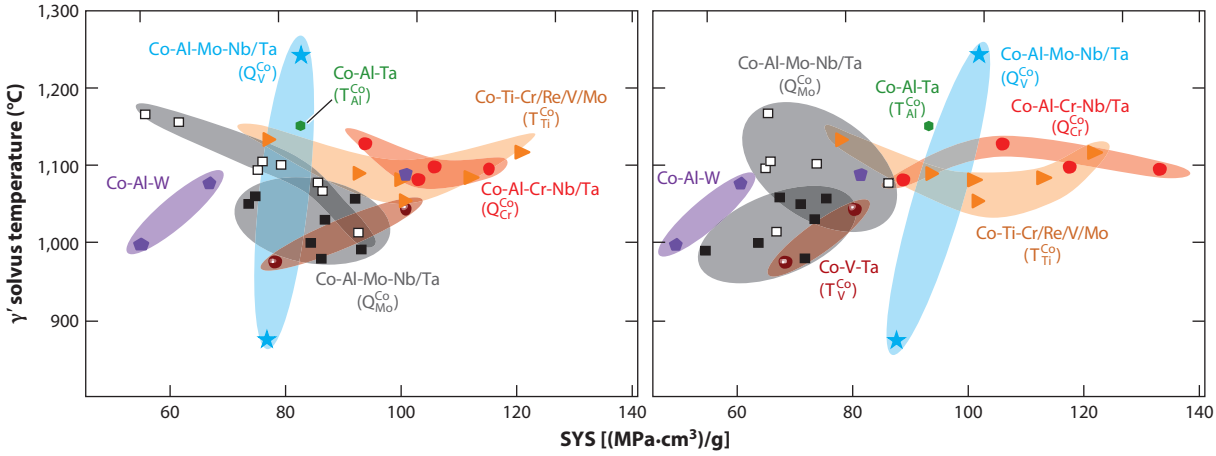

Figure 8

Ashby plots of γ′ solvus temperature (°C) versus 0.2% specific yield stress (SYS) [(MPa·cm^3)/g] at (*a*) room temperature and (*b*) high temperature among the quaternary (Q^{Co}), ternary (T^{Co}), and Co-Al-W base alloys. High temperature is the peak temperature (varies between 650°C and 870°C) at which the particular alloy exhibits a peak value of 0.2% SYS. Data from References 11, 15, 16, 18, 19, 23, 24, 29, 31, 36, 42, and 51; P. Pandey, N. Majumdar, M.P. Singh, C. Patil, A. Sharma, et al., unpublished manuscript).

constriction before cross-slipping (51, 69). Hence, to increase the strength at intermediate temperatures, alloying additions should be made that increase the CSF energy and reduce the onset temperature for YSA and increase the γ′ solvus. Additions of Ni, Ta, and Ti to the Co-Al-W base alloy were found to be most effective, as illustrated in the case of the $(Co,Ni)_3(Al,W,Ti,Ta)$ $L1_2$ phase (**Figure 7*c***) (71). Since Ni, Ta, and Ti enhance the high-temperature γ′ stability in a low-density class of alloys, as reported in Section 2.3, similar YSA behavior is also expected. For example, the impact of these three solutes on the YSA behavior was observed in Co-Al-V base (Q^{Co}_V and T^{Co}_V) alloys. In Co-30Ni-10Al-5V-2Nb, Singh et al. (19) observed a decrease in 0.2% YS up to 600°C before an anomalous increase at 800°C, followed by a rapid decrease (**Figure 7*a***). However, in the Co-30Ni-10Al-5V-4Ta-2Ti alloy (Nb replaced with a higher concentration of Ta and Ti), the increase in the YS could be observed from room temperature to 500°C, followed by a rapid increase until 700°C. This is followed by a sharp decrease at higher temperatures (23). The entire trend is similar to the behavior of Ni_3Al-strengthened Ni base alloys (**Figure 7*c***).

Figure 8 shows the Ashby plots of the γ′ solvus versus 0.2% specific YS (SYS) [(MPa·cm^3)/g] for the low-density Co base superalloys (both Q^{Co} and T^{Co}) at room temperature and high temperature. The data for the Co-Al-W base superalloys were also included. High temperature represents the temperature (varies between 650°C and 870°C) at which the particular alloy exhibits a peak value of 0.2% YS. At room temperature, some of the low-density alloy compositions from Q^{Co}_V, Q^{Co}_{Cr}, and T^{Co}_{Ti} have 0.2% SYS values >100 (MPa·cm^3)/g as well as γ′ solvus temperatures exceeding 1,100°C. For example, Co-30Ni-7Al-12Cr-2Ta-4Ti-0.006B (Q^{Co}_{Cr}) (P. Pandey, N. Majumdar, A. Sharma, D. Palanisamy, S.K. Makineni, et al., unpublished manuscript) shows 0.2% SYS values of ∼103 and ∼115 (MPa·cm^3)/g at room and high (870°C) temperatures, respectively, with a γ′ solvus of ∼1,100°C. This represents one of the best combinations of SYS and high-temperature capability among this class of alloys. Another promising alloy composition is Co-30Ni-10Al-5V-4Ta-2Ti (T^{Co}_V), which exhibits a γ′ solvus of 1,243°C with SYS > 80 (MPa·cm^3)/g at both room and high (700°C) temperatures (23).

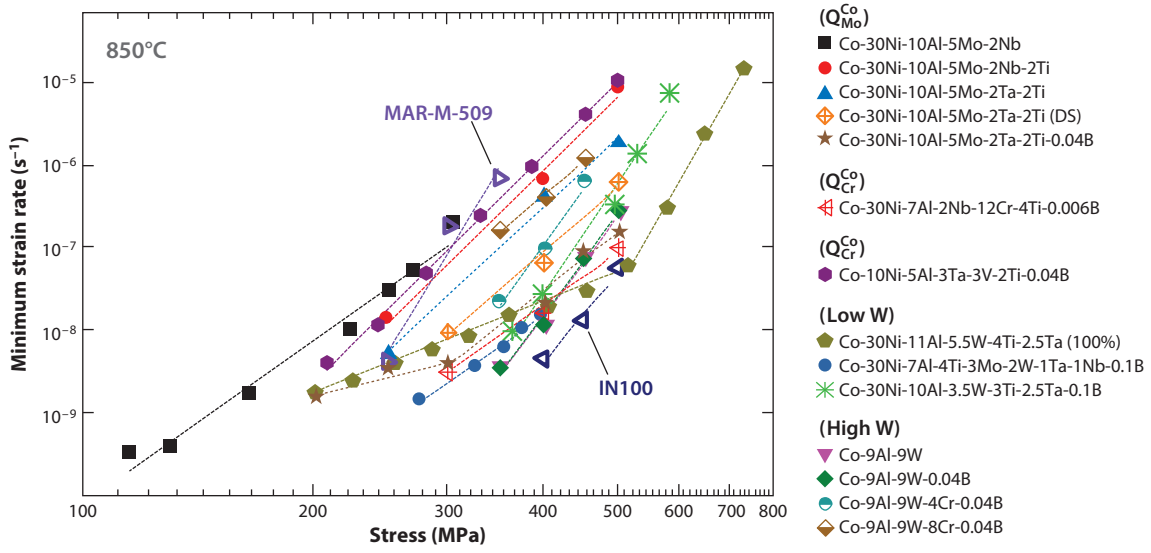

Figure 9

Minimum creep strain at 850°C is plotted as a function of applied stress for some of the low-density Co base superalloys compared with Co-Al-W base, low W–containing Co-Al-W base, and Ni base superalloys. Creep resistance of all γ′-strengthened Co base superalloys primarily lies between MAR-M-509 (Co base solid-solution-strengthened superalloy) and IN100 (Ni base superalloy). Data from References 43, 48, 57, 71, 74, 76, and 77; P. Pandey, N. Majumdar, A. Sharma, D. Palanisamy, S.K. Makineni, et al., unpublished manuscript; A. Sharma, C. Mondal, S.K. Makineni, D. Banerjee & K. Chattopadhyay, unpublished manuscript.

3.2. Creep Properties

Reports on the creep behavior of the low-density Co base alloys are limited. **Figure 9** shows the plots of minimum creep rates versus stress at 850°C for some of the low-density alloys compared with a Co base solid-solution-strengthened alloy (MAR-M-509), Co-Al-W base alloys, and a Ni base alloy (IN100). Microstructural analysis after compressive creep deformation of the Co-30Ni-10Al-5Mo-2Nb (Q^{Co}_{Mo}) alloy (γ′ volume fraction of 35%) at 850°C (63) reveals directional coarsening of the γ′ phase perpendicular to the compressive load direction due to the positive γ/γ′ lattice misfit. Sharma (74) also observed extensive grain boundary decohesion in a postcreep microstructure in a similar Co-30Ni-10Al-5Mo-2Nb-2Ti (Q^{Co}_{Mo}) alloy. This indicates the occurrence of intergranular failure during creep deformation of this class of alloys. Bauer et al. (9, 75) also reported decohesion of the grain boundaries in Co-Al-W base alloys that resulted in creep failure at an early stage and, hence, inferior creep behavior compared to the polycrystalline Ni base superalloys. In Co-Al-W base alloys, the addition of grain boundary strengtheners such as B and Zr leads to the formation of W and Co borides along the grain boundaries (13). These borides reduced the creep rates significantly, and the properties become comparable to those of Ni base IN-713C and IN-100 alloys (13). Recently, Sharma (74) investigated the effect of B (0.04 at%) in Co-30Ni-10Al-5Mo-2Ta-2Ti (Q^{Co}_{Mo}) and showed a significant improvement in creep resistance (**Figure 9**). Hence, creep properties for most of the low-density Co base alloys were evaluated for B-added alloys such as for Co-10Ni-5Al-3Ta-3V-2Ti-0.04B (T^{Co}_{V}) (76) and Co-30Ni-7Al-2Nb-12Cr-4Ti-0.006B (Q^{Co}_{Cr}) (P. Pandey, N. Majumdar, A. Sharma, D. Palanisamy, S.K. Makineni, et al., unpublished manuscript) alloys.

Optimization of alloy mass density with improved creep properties is a current objective among researchers. For example, the density of the Co-10Ni-5Al-3Ta-3V-2Ti-0.04B (T^{Co}_{V}) alloy was measured to be 8.59 g/cm^3, higher by 0.47 g/cm^3 compared to the Co-30Ni-10Al-5Mo-2Nb

alloy that exhibits a similar γ′ creep behavior (76). Reyes Tirado et al. (78) replaced Ta with Nb and increased the Ti by 4 at% in the former alloy, which led to an alloy with the composition Co-10Ni-5Al-3Nb-3V-6Ti-0.04B (T_V^{Co}). Although this alloy exhibits a lower density of 7.97 g/cm^3, the creep rate also reduces by a factor of 1.75, and it shows lower creep resistance than Co-9Al-9W base alloys (43). Another approach to optimization was by reducing the W in Co-9Al-9W base alloys. Lass et al. (57) replaced varying amounts of W with Mo/Nb. The alloy Co-30Ni-7Al-4Ti-2W-3Mo-1Nb-1Ta-0.1B has a density of 8.89 g/cm^3, a higher γ′ volume fraction (∼78%), and comparable creep properties to Co-9Al-9W-0.04B (**Figure 9**). Among alloying additions, Cr tends to reduce the creep rate and density further. For example, a twofold reduction in creep rate occurred after Cr (8 at%) addition in the Co-30Ni-7Al-4Ti-2W-3Mo-1Nb-1Ta-0.1B alloy and made it lighter by ∼0.11 g/cm^3 (79). Similarly, in the Co-10Ni-5Al-3Nb-3V-6Ti-0.04B (T_V^{Co}) alloy, replacement of 4 at% Ti by Cr enhanced the creep resistance (78). In contrast, Cr addition to the Co-9Al-9W-0.04B alloy resulted in deteriorated creep properties (43). The difference was attributed to the presence of Ni in the low-density Co base alloys that increases the Cr partitioning into the γ matrix phase and hence enhances the efficacy of solid-solution strengthening (67, 71). Recently, an alloy was developed with the composition Co-10Ni-7Al-2Nb-12Cr-4Ti-0.006B (Q_{Cr}^{Co}) that shows comparable creep resistance to Co-9Al-9W base alloys and has a mass density as low as 8.08 g/cm^3 (P. Pandey, N. Majumdar, A. Sharma, D. Palanisamy, S.K. Makineni, et al., unpublished manuscript). **Figure 9** reveals that the creep resistance of the present low-density alloys is higher than that of MAR-M-509 (Co base solid-solution-strengthened alloy), and some of them are closer to that of IN100 (Ni base superalloy).

Most of these new Co base alloys show a high-stress exponent (n) $\gtrsim$6.5 at high stress levels. However, in a recent study on the directionally solidified Co-30Ni-10Al-5Mo-2Ta-2Ti (Q_{Mo}^{Co}) alloy, a significant reduction in the stress exponent (<4) at low stress levels (200–400 MPa) was also observed (**Figure 9**). A similar change in stress exponent as a function of creep stress occurs in W-containing $L1_2$ single-phase $(Co,Ni)_3(Al,W,Ti,Ta)$ in the Co-30Ni-10Al-3.5W-3Ti-2.5Ta-0.1B alloy (71). This difference in stress exponent values indicates the change in the creep deformation mechanism. More specifically, it demonstrates the dislocation creep by shearing of γ′ precipitates at high stress levels and diffusional creep at low stress levels (A. Sharma, C. Mondal, S.K. Makineni, D. Banerjee & K. Chattopadhyay, unpublished manuscript).

4. OXIDATION PROPERTIES

Klein et al. (80–82) and Weiser et al. (83, 84) reported extensive oxidation studies on Co-Al-W base systems. The recently developed low-W and Co-Al-Mo (Q_{Mo}^{Co}) base superalloys have also been evaluated for their oxidation kinetics and mechanism (85–87). The development of oxidation-resistant alloys demands a slow-growing, continuous α-Al_2O_3 layer on the alloy surface. Therefore, it is essential to understand the evolution of the Al_2O_3 barrier layer in the presence of different solutes.

Higher W content promotes Al_2O_3 layer formation. However, the depletion of Al was reported to destabilize the γ/γ′ microstructure below the Al_2O_3 layer, leading to the formation of the Co_3W phase in the γ matrix during oxidation (88). Stewart et al. (85) and Forsik et al. (87) studied the low W–containing Co superalloys, emphasizing the need for improving oxidation at 1,100°C. Using both experimental and computational tools, Stewart et al. (86) arrived at the alloy composition Co-36.5Ni-13.2Al-1W-6Cr-3.5Ta, which can form a continuous Al_2O_3 scale at 1,100°C from the early stage of oxidation. However, the performance of these alloys needs to be evaluated at 800°C and 900°C, where alumina formation is usually sluggish.

Moskal and coworkers (89–91) performed preliminary oxidation experiments in air on Co-20Ni-10Al-5Mo-2Nb (Q_{Mo}^{Co}) superalloys. The continuous mass gain curves while heating the

samples from room temperature to 1,200°C indicate that Ni addition improves the oxidation resistance. However, no underlying reasons were suggested. A similar improvement was also reported for Co-Ni-Al-W superalloys (81), in which it was proposed that Ni enhances the Al diffusivity, promoting the early formation of the Al_2O_3 scale. Migas et al. (90) also studied the cyclic oxidation behavior of Co-10Al-5Mo-2Nb and Co-9Al-9W alloys at 800°C. The oxides were thin and intact in the case of the Co-9Al-9W superalloy, while severe spallation was observed for the Co-10Al-5Mo-2Nb superalloy.

Das et al. (92) carried out oxidation studies on the Co-30Ni-10Al-5Mo-2Ta (Q^{Co}_{Mo}) alloy at temperatures of 650°C, 700°C, and 800°C. Contrary to the previous studies, oxidation was carried out isothermally for a maximum of 100 h. Spallation remained the critical issue at 800°C. Addition of Ti improved the adherence and stability of the oxide, reducing the oxidation rate (93). Cr is known to facilitate the formation of α-Al_2O_3 and Cr_2O_3 or $CoCr_2O_4$ scale, which essentially blocks the oxidation at elevated temperatures. In another study, Das et al. (93) found that 8 at% Cr is the threshold above which thin and slow-growing scales are formed. Oxidation studies performed on Co-Al-W-(Cr) alloys revealed a similar result (94). Consistent with these observations, the oxidation studies on the Co-30Ni-10Al-4Mo-3Ta-10Cr (Q^{Co}_{Mo}) alloy for 100 h at 800°C indicate formation of a thin oxide scale of ∼500 nm (95). Cr (4 and 8 at%) addition to the Co-10Ni-5Al-3Nb-3V-6Ti-0.04B (T^{Co}_{V}) alloy also reduces the surface oxide thickness and the parabolic growth rate constant at 850°C (78). Although no evidence of the formation of either Al_2O_3 or Cr_2O_3 could be observed in the latter case, the reason for the improvement in oxidation resistance was not explored. It was proposed that an increase of Al and Cr in the alloy can induce the formation of Al_2O_3 or Cr_2O_3 layers. However, a higher Cr composition in the alloys can also promote the formation of deleterious TCP phases (39, 95), thus imposing a limitation on the amount that can be added. **Figure 10*a*,*b*** schematically compares the oxidation mechanisms occurring in Co-Al-W and Co-Al-Mo-Ta-(Ti,Cr) (Q^{Co}_{Mo}) superalloys. The oxide scale developed during 800°C and 900°C oxidation can be primarily divided into three regimes: (*a*) an outer layer consisting of (Co,Ni)O and Co_3O_4, (*b*) an intermediate layer containing oxides of constitutive elements, and (*c*) an innermost layer containing different allotropes of Al_2O_3 (κ- or α-phase) (93). Both classes of alloys showed γ′-denuded zones below the Al_2O_3 layer. During oxidation, these zones contain precipitates of Co_3W (DO_{19}) or $(Co,Ni)_3(Ta,Mo,Nb)$ (DO_a-orthorhombic) phases. In the presence of Cr and Ti, a large amount of TiN precipitates are found in these γ′-denuded zones. **Figure 10*c*** shows a comparison of mass gain for a different class of γ′-strengthened Co base superalloys that show better oxidation resistance.

5. HOT WORKABILITY

Studies on the thermomechanical processing behavior of the low-density alloys have only been carried out in Q^{Co}_{Mo} base and Q^{Co}_{Cr} base compositions of Co-30Ni-10Al-5Mo-2Ta-2Ti-5Cr (96) and Co-30Ni-10Al-2Nb-4Ti-12Cr (97) alloys. Both alloys show a strong dependence of compressive hot deformation behavior on temperature and strain rate. For the former alloy, the optimum regime for hot working was found to be between 1,187°C and 1,225°C at strain rates of 0.001 to 0.5 s^{-1} with a high strain rate sensitivity value of $m = 0.3$. The deformed microstructure in this regime indicates extensive grain recrystallization by a discontinuous dynamic recrystallization mechanism. At higher strain rates (>1 s^{-1}), the strain rate sensitivity was measured to be $m < 0.1$ between 1,125°C and 1,225°C. Deformed microstructure reveals a large degree of grain boundary cracking, cavitation, adiabatic shear bands, and localized plastic flow, indicating an unstable regime of hot working for the alloy. Similar hot deformation behavior was also observed in Co-30Ni-10Al-2Nb-4Ti-12Cr in the temperature region of 1,025°C to 1,175°C.

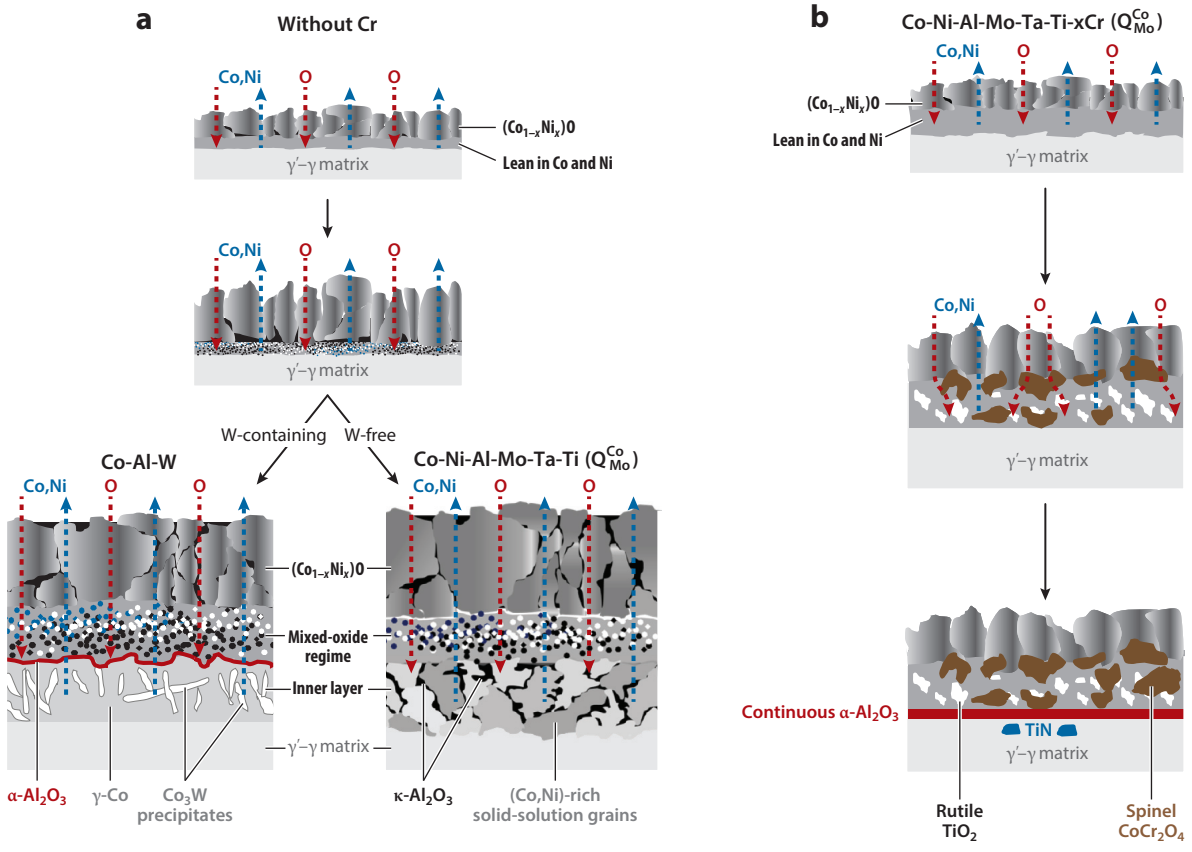

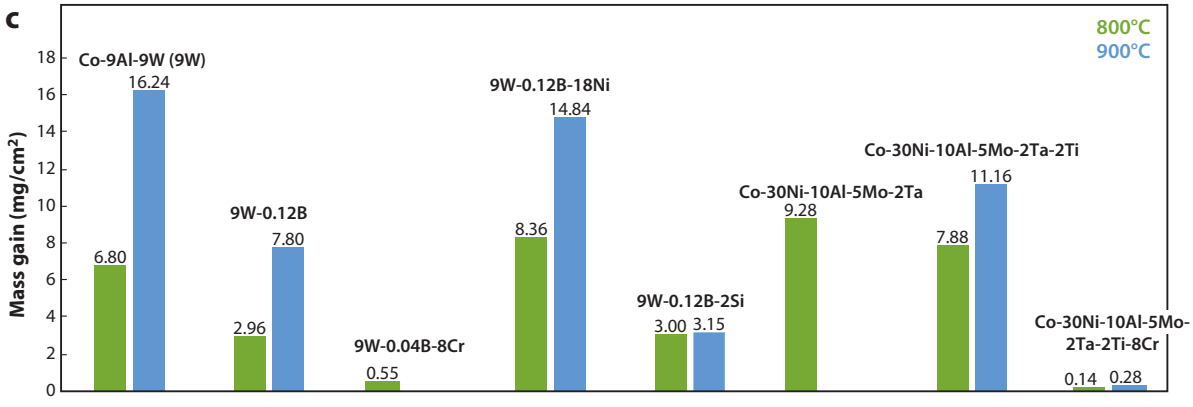

Figure 10

The sequence of events during the oxidation of (*a*) Co-30Ni-10Al-5Mo-2Ta-2Ti and Co-Al-W base superalloys and (*b*) Co-30Ni-10Al-5Mo-2Ta-2Ti-xCr is schematically illustrated, showing the beneficial effect of Cr addition on the formation of continuous alumina scale. (*c*) Comparison of mass gain values for W-containing and W-free Co base superalloys at 800°C and 900°C for 100 h. Data from References 80–82, 92, and 93.

6. FUTURE PROSPECTS

In the last 15 years, significant progress has been made in γ/γ′ Co base superalloys, especially in the Co-Al-W system. One of the main challenges was to reduce its high mass densities (>9.5 g/cm^3). With the discovery of γ/γ′ in Co-Al-Mo-Nb/Ta base alloys in 2015 (14), the field witnessed rapid growth in the design of new γ/γ′ Co base compositions with low mass densities between 7.8 and 8.5 g/cm^3. An attractive recent addition is V-containing alloys that show good physical and mechanical properties. We believe many of these low-density alloys can compete with, and some of them can also supersede, Ni base and Co-Al-W superalloys. However, the hunt for new compositions is not over, and we anticipate more potential Co base alloys with a better combination of high-temperature properties to be found.

There are two critical domains in which the low-density γ/γ′ Co base alloys may play a crucial role. First, the alloys may be used for medium high-temperature range (500–750°C) applications such as in advanced ultrasupercritical power generation systems and chemical plants. Here, the alloys with high SYS are promising, provided they attain superior environmental resistance under the supercritical steam and corrosive gases. The other potential use is in the aviation sector. The Co base solid-solution alloys are already in use in high-temperature sections of gas turbines in which the strength requirement is not critical. With the possibility of strengthening by γ′ precipitates, the use of these new classes of alloys in gas turbine applications may be widened.

Future developments must focus on overcoming the cost barrier inherent to the base Co metal. This requires expanding the potential for high SYS and environmental degradation resistance of the alloys at high temperatures. Presently, we have limited knowledge of the factors that control the oxidation and hot corrosion of these alloys. Further experiments are essential in this direction, primarily on the optimization of Cr composition in the new alloys and exploration of other alloying elements that can enhance oxidation and hot corrosion resistance. Research is also needed on the efficacy of high-temperature bond coats on these alloys.

Knowledge of polycrystalline alloys processing will determine how these alloys will increase the demand for future technologies. Since these new Co base alloys are recent discoveries, no data are available on single-crystal alloys and their behavior at higher temperatures. Hence, we expect significant efforts to explore the long-term creep and fatigue behavior of single-crystal and directionally solidified alloys at high temperatures. The current pace of development of these Co base alloys is impressive and is promising for the advancement of high-performance Co base superalloys in the future.

DISCLOSURE STATEMENT

The authors are not aware of any affiliations, memberships, funding, or financial holdings that might be perceived as affecting the objectivity of this review.

ACKNOWLEDGMENTS

The authors would like to acknowledge fruitful discussions with Professor Dipankar Banerjee. The authors also acknowledge the microscopy and atom probe tomography (APT) facility available at the Advanced Facility for Microscopy and Microanalysis, Indian Institute of Science, Bangalore. K.C. is grateful for financial support from the Department of Science and Technology in the form of a Science and Engineering Research Board Distinguished Fellowship. K.C. and S.K.M. also acknowledge the Gas Turbine Materials and Processes program of the Aeronautics Research and Development Board, Defence Research and Development Organisation, for financial support.

LITERATURE CITED

1. Lee CS. 1971. *Precipitation-hardening characteristics of ternary cobalt-aluminum-X alloys*. PhD thesis, Univ. Ariz., Tucson, AZ
2. Sato J, Omori T, Oikawa K, Ohnuma I, Kainuma R, Ishida K. 2006. Cobalt-base high-temperature alloys. *Science* 312(5770):90–91
3. Mughrabi H. 2014. The importance of sign and magnitude of γ/γ′ lattice misfit in superalloys—with special reference to the new γ′-hardened cobalt-base superalloys. *Acta Mater*. 81:21–29
4. Kobayashi S, Tsukamoto Y, Takasugi T, Chinen H, Omori T, et al. 2009. Determination of phase equilibria in the Co-rich Co–Al–W ternary system with a diffusion-couple technique. *Intermetallics* 17(12):1085–89
5. Feng G, Li H, Li SS, Sha JB. 2012. Effect of Mo additions on microstructure and tensile behavior of a Co–Al–W–Ta–B alloy at room temperature. *Scr. Mater.* 67(5):499–502
6. Chen M, Wang C-Y. 2009. First-principles investigation of the site preference and alloying effect of Mo, Ta and platinum group metals in γ′-Co_3(Al, W). *Scr. Mater.* 60(8):659–62
7. Yan H-Y, Vorontsov VA, Dye D. 2014. Alloying effects in polycrystalline γ′ strengthened Co–Al–W base alloys. *Intermetallics* 48:44–53
8. Yan H-Y, Coakley J, Vorontsov VA, Jones NG, Stone HJ, Dye D. 2014. Alloying and the micromechanics of Co–Al–W–X quaternary alloys. *Mater. Sci. Eng. A* 613:201–8
9. Bauer A, Neumeier S, Pyczak F, Göken M. 2010. Microstructure and creep strength of different γ/γ′-strengthened Co-base superalloy variants. *Scr. Mater.* 63(12):1197–200
10. Knop M, Mulvey P, Ismail F, Radecka A, Rahman KM, et al. 2014. A new polycrystalline Co-Ni superalloy. *JOM* 66(12):2495–501
11. Neumeier S, Freund LP, Göken M. 2015. Novel wrought γ/γ′ cobalt base superalloys with high strength and improved oxidation resistance. *Scr. Mater.* 109:104–7
12. Shi L, Yu JJ, Cui CY, Sun XF. 2015. Microstructural stability and tensile properties of a Ti-containing single-crystal Co–Ni–Al–W–base alloy. *Mater. Sci. Eng. A* 646:45–51
13. Bocchini PJ, Sudbrack CK, Noebe RD, Dunand DC, Seidman DN. 2017. Microstructural and creep properties of boron- and zirconium-containing cobalt-based superalloys. *Mater. Sci. Eng. A* 682:260–69
14. Makineni SK, Nithin B, Chattopadhyay K. 2015. A new tungsten-free γ–γ′ Co–Al–Mo–Nb-based superalloy. *Scr. Mater.* 98:36–39
15. Makineni SK, Samanta A, Rojhirunsakool T, Alam T, Nithin B, et al. 2015. A new class of high strength high temperature Cobalt based γ–γ′ Co–Mo–Al alloys stabilized with Ta addition. *Acta Mater*. 97:29–40
16. Makineni SK, Nithin B, Chattopadhyay K. 2015. Synthesis of a new tungsten-free γ–γ′ cobalt-based superalloy by tuning alloying additions. *Acta Mater*. 85:85–94
17. Makineni SK, Nithin B, Palanisamy D, Chattopadhyay K. 2016. Phase evolution and crystallography of precipitates during decomposition of new "tungsten-free" Co(Ni)–Mo–Al–Nb γ–γ′ superalloys at elevated temperatures. *J. Mater. Sci.* 51(17):7843–60
18. Pandey P, Mukhopadhyay S, Srivastava C, Makineni SK, Chattopadhyay K. 2020. Development of new γ′-strengthened Co-based superalloys with low mass density, high solvus temperature and high temperature strength. *Mater. Sci. Eng. A* 790:139578
19. Singh MP, Makineni SK, Chattopadhyay K. 2020. Achieving lower mass density with high strength in Nb stabilised γ/γ′ Co–Al–Mo–Nb base superalloy by the replacement of Mo with V. *Mater. Sci. Eng. A* 794:139826
20. Yao Q, Shang S-L, Hu Y-J, Wang Y, Wang Y, et al. 2016. First-principles investigation of phase stability, elastic and thermodynamic properties in $L1_2$ Co_3(Al,Mo,Nb) phase. *Intermetallics* 78:1–7
21. Tanaka K, Ohashi T, Kishida K, Inui H. 2007. Single-crystal elastic constants of Co_3 (Al, W) with the $L1_2$ structure. *Appl. Phys. Lett.* 91(18):181907
22. Omori T, Oikawa K, Sato J, Ohnuma I, Kattner UR, et al. 2013. Partition behavior of alloying elements and phase transformation temperatures in Co–Al–W–base quaternary systems. *Intermetallics* 32:274–83
23. Chen Y, Wang C, Ruan J, Omori T, Kainuma R, et al. 2019. High-strength Co–Al–V-base superalloys strengthened by γ′-Co_3(Al,V) with high solvus temperature. *Acta Mater*. 170:62–74

24. Chen Y, Wang C, Ruan J, Yang S, Omori T, et al. 2020. Development of low-density γ/γ′ Co–Al–Ta-based superalloys with high solvus temperature. *Acta Mater*. 188:652–64
25. Murray JL. 1982. The Co−Ti (cobalt−titanium) system. *Bull. Alloy Phase Diagr.* 3(1):74
26. Bhowmik A, Neumeier S, Rhode S, Stone HJ. 2015. Allotropic transformation induced stacking faults and discontinuous coarsening in a γ-γ′ Co-base alloy. *Intermetallics* 59:95–101
27. Blaise JM, Viatour P, Drapier JM. 1970. On the stability and precipitation of the Co_3Ti phase in Co-Ti alloys. *Cobalt* 49:192–95
28. Viatour P, Drapier JM, Coutsouradis D. 1973. Stability of the gamma prime-Co_3Ti compound in simple and complex cobalt alloys. *Cobalt* 3:67–74
29. Zenk CH, Povstugar I, Li R, Rinaldi F, Neumeier S, et al. 2017. A novel type of Co–Ti–Cr-base γ/γ′ superalloys with low mass density. *Acta Mater*. 135:244–51
30. Im HJ, Makineni SK, Gault B, Stein F, Raabe D, Choi P-P. 2018. Elemental partitioning and site-occupancy in γ/γ′ forming Co-Ti-Mo and Co-Ti-Cr alloys. *Scr. Mater.* 154:159–62
31. Im HJ, Lee S, Choi WS, Makineni SK, Raabe D, et al. 2020. Effects of Mo on the mechanical behavior of γ/γ′-strengthened Co-Ti-based alloys. *Acta Mater*. 197:69–80
32. Ruan JJ, Wang CP, Zhao CC, Yang SY, Yang T, Liu XJ. 2014. Experimental investigation of phase equilibria and microstructure in the Co-Ti-V ternary system. *Intermetallics* 49:121–31
33. Yoo B, Im HJ, Seol J-B, Choi P-P. 2019. On the microstructural evolution and partitioning behavior of $L1_2$-structured γ′-based Co-Ti-W alloys upon Cr and Al alloying. *Intermetallics* 104:97–102
34. Nyshadham C, Oses C, Hansen JE, Takeuchi I, Curtarolo S, Hart GL. 2017. A computational high-throughput search for new ternary superalloys. *Acta Mater*. 122:438–47
35. Reyes Tirado FL, Perrin Toinin J, Dunand DC. 2018. γ+γ′ microstructures in the Co-Ta-V and Co-Nb-V ternary systems. *Acta Mater*. 151:137–48
36. Ruan J, Xu W, Yang T, Yu J, Yang S, et al. 2020. Accelerated design of novel W-free high-strength Co-base superalloys with extremely wide γ/γ′ region by machine learning and CALPHAD methods. *Acta Mater*. 186:425–33
37. Mukhopadhyay S, Pandey P, Baler N, Biswas K, Makineni SK, Chattopadhyay K. 2021. The role of Ti addition on the evolution and stability of γ/γ′ microstructure in a Co-30Ni-10Al-5Mo-2Ta alloy. *Acta Mater*. 208:116736
38. Pandey P, Sawant AK, Nithin B, Peng Z, Makineni SK, et al. 2019. On the effect of Re addition on microstructural evolution of a CoNi-based superalloy. *Acta Mater*. 168:37–51
39. Nithin B, Samanta A, Makineni SK, Alam T, Pandey P, et al. 2017. Effect of Cr addition on γ–γ′ cobalt-based Co–Mo–Al–Ta class of superalloys: a combined experimental and computational study. *J. Mater. Sci.* 52(18):11036–47
40. Pandey P, Makineni SK, Samanta A, Sharma A, Das SM, et al. 2019. Elemental site occupancy in the $L1_2$ A_3B ordered intermetallic phase in Co-based superalloys and its influence on the microstructure. *Acta Mater*. 163:140–53
41. Baler N, Pandey P, Singh MP, Makineni SK, Chattopadhyay K. Effects of Ti and Cr additions in a Co-Ni-Al-Mo-Nb based superalloy. In *Superalloys 2020*, ed. S Tin, M Hardy, J Clews, J Cormier, Q Feng, et al., pp. 929–36. Cham, Switz.: Springer
42. Li L, Wang C, Chen Y, Yang S, Yang M, et al. 2019. Effect of Re on microstructure and mechanical properties of γ/γ′ Co-Ti-based superalloys. *Intermetallics* 115:106612
43. Povstugar I, Zenk CH, Li R, Choi P-P, Neumeier S, et al. 2016. Elemental partitioning, lattice misfit and creep behaviour of Cr containing γ′ strengthened Co base superalloys. *Mater. Sci. Technol.* 32(3):220–25
44. Povstugar I, Choi P-P, Neumeier S, Bauer A, Zenk CH, et al. 2014. Elemental partitioning and mechanical properties of Ti- and Ta-containing Co–Al–W-base superalloys studied by atom probe tomography and nanoindentation. *Acta Mater*. 78:78–85
45. Shinagawa K, Omori T, Sato J, Oikawa K, Ohnuma I, et al. 2008. Phase equilibria and microstructure on γ′ phase in Co-Ni-Al-W system. *Mater. Trans.* 49(6):1474–79
46. Volz N, Zenk CH, Cherukuri R, Kalfhaus T, Weiser M, et al. 2018. Thermophysical and mechanical properties of advanced single crystalline Co-base superalloys. *Metall. Mater. Trans. A* 49(9):4099–109
47. Kolb M, Zenk CH, Kirzinger A, Povstugar I, Raabe D, et al. 2017. Influence of rhenium on γ′-strengthened cobalt-base superalloys. *J. Mater. Res.* 32(13):2551–59

48. Liu Q, Coakley J, Seidman DN, Dunand DC. 2016. Precipitate evolution and creep behavior of a W-free Co-based superalloy. *Metall. Mater. Trans. A* 47(12):6090–96
49. Ruan JJ, Liu XJ, Yang SY, Xu WW, Omori T, et al. 2018. Novel Co-Ti-V-base superalloys reinforced by $L1_2$-ordered γ′ phase. *Intermetallics* 92:126–32
50. Zhuang X, Lu S, Li L, Feng Q. 2020. Microstructures and properties of a novel γ′-strengthened multi-component CoNi-based wrought superalloy designed by CALPHAD method. *Mater. Sci. Eng. A* 780:139219
51. Suzuki A, Inui H, Pollock TM. 2015. $L1_2$-strengthened cobalt-base superalloys. *Annu. Rev. Mater. Res.* 45:345–68
52. Calderon HA, Voorhees PW, Murray JL, Kostorz G. 1994. Ostwald ripening in concentrated alloys. *Acta Metall. Mater.* 42(3):991–1000
53. Sauza DJ, Bocchini PJ, Dunand DC, Seidman DN. 2016. Influence of ruthenium on microstructural evolution in a model Co–Al–W superalloy. *Acta Mater*. 117:135–45
54. Azzam A, Philippe T, Hauet A, Danoix F, Locq D, et al. 2018. Kinetics pathway of precipitation in model Co-Al-W superalloy. *Acta Mater*. 145:377–87
55. Meher S, Nag S, Tiley J, Goel A, Banerjee R. 2013. Coarsening kinetics of γ′ precipitates in cobalt-base alloys. *Acta Mater*. 61(11):4266–76
56. Baler N, Pandey P, Palanisamy D, Makineni SK, Phanikumar G, Chattopadhyay K. 2020. On the effect of W addition on microstructural evolution and γ′ precipitate coarsening in a Co–30Ni–10Al–5Mo–2Ta–2Ti alloy. *Materialia* 10:100632
57. Lass EA, Grist RD, Williams ME. 2016. Phase equilibria and microstructural evolution in ternary Co-Al-W between 750 and 1100°C. *J. Phase Equilib. Diffus.* 37(4):387–401
58. Hadjiapostolidou D, Shollock BA. 2008. Long term coarsening in René 80 Ni-base superalloy. *Superalloys* 2008:733–739
59. Footner PK, Richards BP. 1982. Long—term growth of superalloy γ′ particles. *J. Mater. Sci.* 17(7):2141–53
60. MacKay RA, Nathal MV. 1990. γ′ coarsening in high volume fraction nickel-base alloys. *Acta Metall. Mater.* 38(6):993–1005
61. MacKay RA, Ebert LJ. 1983. The development of directional coarsening of the γ′ precipitate in superalloy single crystals. *Scr. Metall.* 17(10):1217–22
62. Miyazaki T, Imamura H, Kozakai T. 1982. The formation of "γ′ precipitate doublets" in Ni•Al alloys and their energetic stability. *Mater. Sci. Eng.* 54(1):9–15
63. Qu S, Li Y, Wang C, Liu X, Qian K, et al. 2020. Coarsening behavior of γ′ precipitates and compression deformation mechanism of a novel Co–V–Ta–Ti superalloy. *Mater. Sci. Eng. A* 787:139455
64. Takasugi T, Hirakawa S, Izumi O, Ono S, Watanabe S. 1987. Plastic flow of Co_3 Ti single crystals. *Acta Metall*. 35(8):2015–26
65. Liu Y, Takasugi T, Izumi O, Suenaga H. 1989. Mechanical properties of Co_3Ti polycrystals alloyed with various additions. *J. Mater. Sci.* 24(12):4458–66
66. Suzuki A, DeNolf GC, Pollock TM. 2007. Flow stress anomalies in γ/γ′ two-phase Co–Al–W-base alloys. *Scr. Mater.* 56(5):385–88
67. Suzuki A, Pollock TM. 2008. High-temperature strength and deformation of γ/γ′ two-phase Co–Al–W-base alloys. *Acta Mater*. 56(6):1288–97
68. Mishima Y, Ochiai S, Yodogawa M, Suzuki T. 1986. Mechanical properties of Ni_3Al with ternary addition of transition metal elements. *Trans. Jpn. Inst. Metals* 27(1):41–50
69. Okamoto NL, Oohashi T, Adachi H, Kishida K, Inui H, Veyssière P. 2011. Plastic deformation of polycrystals of $Co_3(Al,W)$ with the $L1_2$ structure. *Philos. Mag.* 91(28):3667–84
70. Vamsi KV, Karthikeyan S. 2017. Yield anomaly in $L1_2$ $Co_3Al_xW_{1-x}$ vis-à-vis Ni_3Al. *Scr. Mater.* 130:269–73
71. Long FR, Baik SI, Chung DW, Xue F, Lass EA, et al. 2020. Microstructure and creep performance of a multicomponent Co-based $L1_2$-ordered intermetallic alloy. *Acta Mater*. 196:396–408
72. Vitek V, Paidar V. 2008. Non-planar dislocation cores: a ubiquitous phenomenon affecting mechanical properties of crystalline materials. *Dislocations Solids* 14:439–514
73. Kear BH, Wilsdorf HG. 1962. Dislocation configurations in plastically deformed polycrystalline Cu_3Au alloys. *Trans. Met. Soc. AIME* 224:382

74. Sharma A. 2019. *An evaluation of the mechanical behavior of some new high temperature materials*. PhD Thesis, Indian Inst. Sci., Bangalore, India
75. Bauer A, Neumeier S, Pyczak F, Göken M. 2012. Creep strength and microstructure of polycrystalline γ′-strengthened cobalt-base superalloys. *Superalloys* 12:695–703
76. Reyes Tirado FL, Taylor S, Dunand DC. 2019. Effect of Al, Ti and Cr additions on the γ-γ′ microstructure of W-free Co-Ta-V-based superalloys. *Acta Mater.* 172:44–54
77. Bauer A, Neumeier S, Pyczak F, Singer RF, Göken M. 2012. Creep properties of different γ′-strengthened Co-base superalloys. *Mater. Sci. Eng. A* 550:333–41
78. Reyes Tirado FL, Taylor SV, Dunand DC. 2020. Low-density, W-free Co–Nb–V–Al-based superalloys with γ/γ′ microstructure. *Mater. Sci. Eng. A* 796:139977
79. Ng DS, Chung D-W, Toinin JP, Seidman DN, Dunand DC, Lass EA. 2020. Effect of Cr additions on a γ-γ′ microstructure and creep behavior of a Co-based superalloy with low W content. *Mater. Sci. Eng. A* 778:139108
80. Klein L, Bauer A, Neumeier S, Göken M, Virtanen S. 2011. High temperature oxidation of γ/γ′-strengthened Co-base superalloys. *Corros. Sci.* 53(5):2027–34
81. Klein L, Killian MS, Virtanen S. 2013. The effect of nickel and silicon addition on some oxidation properties of novel Co-based high temperature alloys. *Corros. Sci.* 69:43–49
82. Klein L, Shen Y, Killian MS, Virtanen S. 2011. Effect of B and Cr on the high temperature oxidation behaviour of novel γ/γ′-strengthened Co-base superalloys. *Corros. Sci.* 53(9):2713–20
83. Weiser M, Galetz MC, Zschau H-E, Zenk CH, Neumeier S, et al. 2019. Influence of Co to Ni ratio in γ′-strengthened model alloys on oxidation resistance and the efficacy of the halogen effect at 900°C. *Corros. Sci.* 156:84–95
84. Weiser M, Eggeler YM, Spiecker E, Virtanen S. 2018. Early stages of scale formation during oxidation of γ/γ′ strengthened single crystal ternary Co-base superalloy at 900°. *Corros. Sci.* 135:78–86
85. Stewart CA, Suzuki A, Rhein RK, Pollock TM, Levi CG. 2019. Oxidation behavior across composition space relevant to Co-based γ/γ′ alloys. *Metall. Mater. Trans. A* 50(11):5445–58
86. Stewart CA, Murray SP, Suzuki A, Pollock TM, Levi CG. 2020. Accelerated discovery of oxidation resistant CoNi-base γ/γ′ alloys with high $L1_2$ solvus and low density. *Mater. Des.* 189:108445
87. Forsik SAJ, Polar Rosas AO, Wang T, Colombo GA, Zhou N, et al. 2018. High-temperature oxidation behavior of a novel Co-base superalloy. *Metall. Mater. Trans. A* 49(9):4058–69
88. Weiser M, Virtanen S. 2019. Influence of W content on the oxidation behaviour of ternary γ′-strengthened Co-based model alloys between 800 and 900°C. *Oxid. Met.* 92(5):541–60
89. Moskal G, Tomaszewska A, Mikuszewski T, Maciag T, Godzierz M, Niemiec D. 2017. Oxidation performance of Co–Al–W and Co–Ni–Al–W new type γ–γ′ cobalt-based superalloys. *Mater. Eng.* 4:163–69
90. Migas D, Moskal G, Niemiec D. 2018. Surface condition of new γ–γ′ Co-Al-Mo-Nb and Co-Al-W cobalt-based superalloys after oxidation at 800°C. *J. Mater. Eng. Perform.* 27(2):447–56
91. Moskal G, Migas D, Niemiec D, Tomaszewska A. 2019. Thermogravimetric investigations of novel γ–γ′ Co-Al-W and Co-Al-Mo-Nb cobalt-based superalloys. *J. Eng. Mater. Technol.* 141(4):041008
92. Das SM, Singh MP, Chattopadhyay K. 2019. Evolution of oxides and their microstructures at 800°C in a γ-γ' stabilised Co-Ni-Al-Mo-Ta superalloy. *Corros. Sci.* 155:46–54
93. Das SM, Singh MP, Chattopadhyay K. 2020. Effect of Cr addition on the evolution of protective alumina scales and the oxidation properties of a Ta stabilized γ′-strengthened Co-Ni-Al-Mo-Ta-Ti alloy. *Corros. Sci.* 172:108683
94. Chen Y, Xue F, Wang C, Li X, Deng Q, et al. 2019. Effect of Cr on the microstructure and oxidation properties of Co-Al-W superalloys studied by in situ environmental TEM. *Corros. Sci.* 161:108179
95. Bantounas I, Gwalani B, Alam T, Banerjee R, Dye D. 2019. Elemental partitioning, mechanical and oxidation behaviour of two high-γ′ W-free γ/γ′ polycrystalline Co/Ni superalloys. *Scr. Mater.* 163:44–50
96. Nithin B, Chattopadhyay K, Phanikumar G. 2018. Characterization of the hot deformation behavior and microstructure evolution of a new γ-γ′ strengthened cobalt-based superalloy. *Metall. Mater. Trans. A* 49(10):4895–905
97. Baler N, Pandey P, Chattopadhyay K, Phanikumar G. 2020. Influence of thermomechanical processing parameters on microstructural evolution of a gamma-prime strengthened cobalt based superalloy during high temperature deformation. *Mater. Sci. Eng. A* 791:13949